Atti Accademia Nazionale dei Lincei

Classe Scienze Fisiche Matematiche Naturali

Rendiconti

Cesare Bacci, Corrado Mencuccinì, Gianni Penso, Vittorio Silvestrini, Mario Spinetti, Bruno Stella

Photoproduction of neutral pions in the energy range 400 to 600 MeV of the incident photon

Atti della Accademia Nazionale dei Lincei. Classe di Scienze Fisiche, Matematiche e Naturali. Rendiconti, Serie 8, Vol. **39** (1965), n.6, p. 452–469.

Accademia Nazionale dei Lincei

<http://www.bdim.eu/item?id=RLINA_1965_8_39_6_452_0>

L'utilizzo e la stampa di questo documento digitale è consentito liberamente per motivi di ricerca e studio. Non è consentito l'utilizzo dello stesso per motivi commerciali. Tutte le copie di questo documento devono riportare questo avvertimento.

Articolo digitalizzato nel quadro del programma bdim (Biblioteca Digitale Italiana di Matematica) SIMAI & UMI
http://www.bdim.eu/

Fisica. — *Photoproduction of neutral pions in the energy range 400 to 600 MeV of the incident photon.* Nota di CESARE BACCI (*), CORRADO MENCUCCINI (**), GIANNI PENSO (*), VITTORIO SILVESTRINI (**), MARIO SPINETTI (*) e BRUNO STELLA (**), presentata (***) dal Socio G. SALVINI.

INTRODUCTION.—During the last few years the detailed study of the reactions π + nucleon and γ + nucleon brought to the discovery of a number of strong resonances, which may be considered as excited states of the nucleon [1]. These levels (isobaric states) have a total energy lying between 1236 MeV (first resonance), and 2825 MeV. Among those states, the so called second resonance (total energy 1518 MeV) seems to be somewhat more complicated than indicated by the first measurements. The energy range between the first and the second resonance has become even more interesting as a result of recent experiments. In fact in $\pi - p$ [2], $p - p$ [3] and $K - p$ [4] scattering a more or less evident peak in the cross section was found, at a total center of mass energy of $\sim$ 1410 MeV. The detailed phase-shift analysis carried out in $\pi - p$ scattering [5], shows that the P_{11} phase shift increases at around 1400 MeV total center of mass energy. This suggests the existence of a resonance of mass $\sim$ 1410 MeV and quantum numbers $L = 1$, $T = 1/2$, $J = 1/2$ (P_{11} resonance). The width is of the order of 240 MeV. In fig. 1 the three experimental evidences in favour of the P_{11} resonance ($\pi - p$, $p - p$ and $K - p$ scattering) are shown.

This resonance has not yet been looked for in photoproduction, and therefore an experiment in this direction seems to deserve high interest, in order to get information on the excitation channels of this resonance. The P_{11} resonance could be excited and decay according to the scheme

$$\gamma + p \rightarrow N^*(1410) \rightarrow \pi^0 + p.$$

It should appear in photoproduction at an energy of $\sim$ 590 MeV of the incident photon, with a half width of $\sim \pm$ 120 MeV.

The main difficulty in searching for P_{11} resonance in photoproduction, as in other reaction channels, is the small mass difference between the P_{11} and the second resonance, which is of the same order of the half width of the P_{11} : $\sim$ 100 MeV and $\sim$ 120 MeV respectively.

For the same reason, however, we think that a good knowledge of this energy region is necessary to understand the second resonance.

The experiment described in the following was undertaken in order to give a contribution in this direction.

(*) Istituto di Fisica dell'Università, Roma and INFN, Sezione di Roma.
(**) Laboratori Nazionali del CNEN, Frascati (Roma).
(***) Nella seduta dell'11 dicembre 1965.

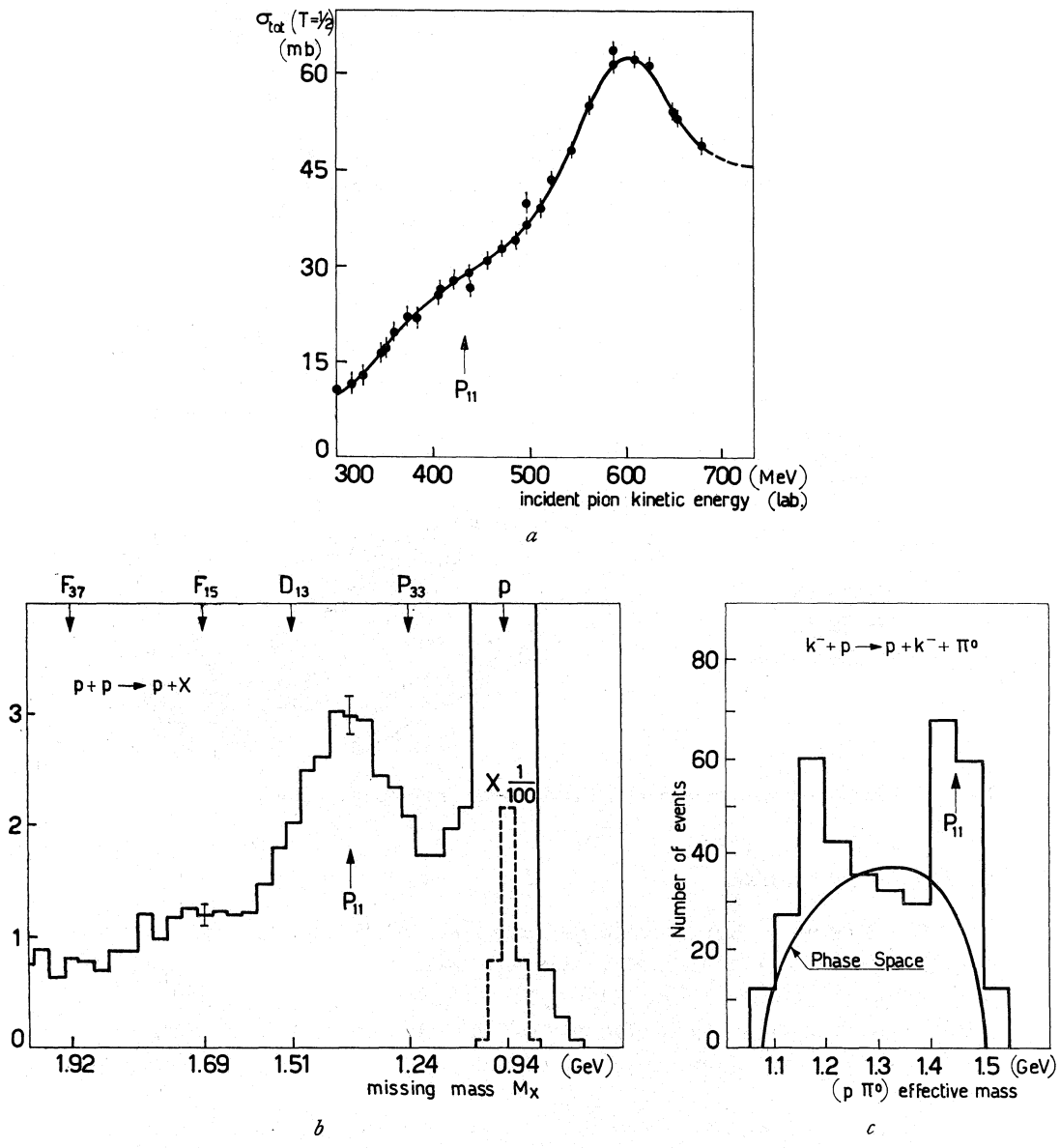


Fig. 1. – Experimental evidences in favour of the P_{11} resonance, from:

a) $\pi - p$ total cross-section in 1/2 isospin state [2];
b) $p - p$ anelastic scattering [3] at 19·3 GeV/*c*;
c) $K + p \to p + K^- + \pi^0$ reaction [4].

EXPERIMENTAL ARRANGEMENT.—The experimental lay-out is shown in fig. 2. The γ-ray beam, produced by bremsstrahlung in a tantalium target of the electrons accelerated by the 1.1 GeV Frascati electron-synchrotron, hits a liquid hydrogen target [6], 7.5 cm thick. A Wilson quantameter [7] measures the beam intensity.

The experimental apparatus is made of a proton telescope (counters and spark chambers) to detect the recoil proton from reaction

(1) $$\gamma + p \rightarrow p + \pi^0$$

and of a γ telescope (lead glass Cerenkov counter with an anticoincidence in front), which detects γ–rays from the π^0 decay and measures their energy. The spark chambers are triggered by a coincidence of a γ–ray with the proton telescope.

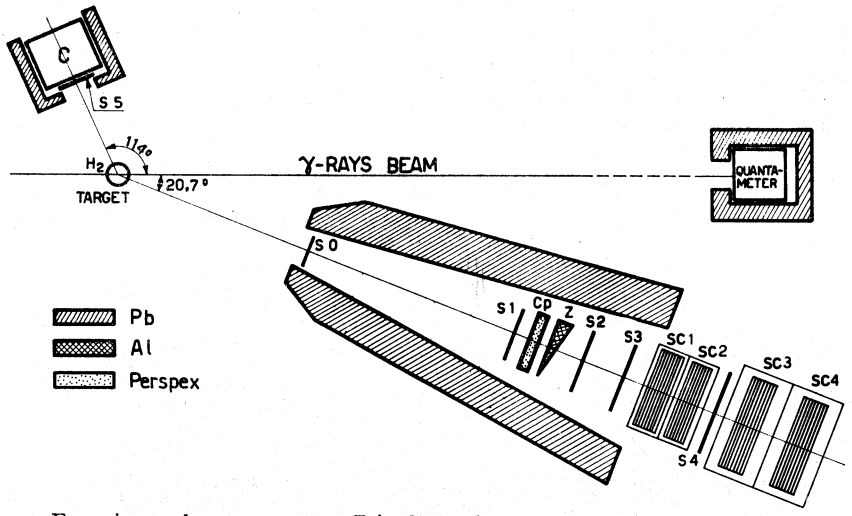


Fig. 2. – Experimental arrangement. Z is the wedge shaped aluminum absorber (see text).

a) *The proton telescope.*

It is formed of five scintillation counters (S_0 , S_1 , S_2 , S_3 , S_4), of a perspex Cerenkov counter (Cp), at an angle of 20°.7 with the γ–rays beam, and of four spark chambers. The solid angle, defined by counter S_3, is 6.7 msr in the laboratory system. The dimensions, the position and the characteristics of the counters and of the absorbers of the proton telescope are summarized in Table I.

All the counters are viewed by a photomultiplier Philips 56 AVP, but counters S_2 and Cp: the first one, on which a pulse height analysis is made, is viewed by two 56 AVP and the second one by four.

The four spark chambers [8] (SC_1 , SC_2 , SC_3 and SC_4) are sandwiches of 13 aluminum plates 3 mm thick and glass frames, 5.5 mm thick, glued with araldite. By a measurement of the energy of the protons through their range, and of the angle of emission of the protons, a resolution of $\sim \pm 1\%$ in the incident photon energy is obtained.

Between Cp and S_2, a wedge shaped aluminum absorber is interposed, to compensate for the dependence of the energy of the protons from reaction (1) on their angle of emission. A one to one correspondence between the stopping

TABLE I.

Characteristics of counters and absorbers.

Distance from H_2 target (cm)	Counter	Material	Dimensions	Phototubes N°	Phototubes Type
		Proton	Telescope		
98		Al plate	8 mm thick		
100	S_0	plastic scintillator	15 × 15 × 0.5 cm^3	1	Philips 56 AVP
215	S_1	plastic scintillator	23 × 23 × 1.25 cm^3	1	Philips 56 AVP
225	Cp	perspex	25 × 25 × 5.6 cm^3	4	Philips 56 AVP
235		Al wedge	12 mm average thickness		
245		Al plate	30 mm thick		
249	S_2	plastic scintillator	23 × 23 × 2.5 cm^3	2	Philips 56 AVP
259		Cu plate	3 mm thick		
269	S_3	plastic scintillator	22 × 22 × 1 cm^3	1	Philips 56 AVP
282 first plate	$CS_1 + CS_2$	(13 + 13) Al plates	(13 + 13) (31.5 × 31.5 × 0.3 cm^3)		
315	S_4	plastic scintillator	35 × 35 × 1.2 cm^3	1	Philips 56 AVP
330 first plate	$CS_3 + CS_4$	(13 + 13) Al plates	(13 + 13) (41.5 × 41.5 × 0.3 cm^3)		
		γ–ray	Telescope		
45	S_5	plastic scintillator	27 × 27 × 1.2 cm^3	1	Philips 56 AVP
50	C	lead glass cylinder	ø 30 cm × 25 cm	3	Philips 58 AVP

gap of the proton and the incident photon energy is thus obtained, simplifying the analysis of the data.

The logic of the experiment will be discussed later, when describing the block diagram of the electronics.

b) *The γ–ray telescope.*

On the line of flight of the π^0 (114^0 respect to the γ–ray beam) there is a total absorption lead glass Cerenkov counter C. It is a glass cylinder, 60% of Pb in weight, 25 cm thick and 30 cm diameter, viewed by three photomultipliers Philips 58 AVP. In front of it, the scintillation counter S_5 in anticoincidence eliminates charged particles.

The pulse height in C is proportional to the energy of the detected γ–ray. The slope of the response of the Cerenkov vs. γ–ray energy is obtained by calibration of the Cerenkov with monochromatic electrons (see Appendix III).

BLOCK DIAGRAM OF THE ELECTRONICS.—The block diagram of the electronics is shown in fig. 3, and its logic will appear clear from the following discussion.

The elimination of charged pions and electrons from the proton channel is obtained as follows:

a) The request of a γ–ray in coincidence with the proton telescope reduces the contamination of pions and electrons from $\sim 5:1$ to $1:2$.

b) The discrimination on S_1, low enough to accept all of the protons, allows pions and electrons to be further rejected. This condition is more efficient for low energy particles.

c) The Cerenkov counter Cp in anticoincidence, allows pions and electrons to be almost completely eliminated from the most energetic particles.

d) The pulse heights in counters S_2 and S_3 are digitized and recorded in binary form by means of neon lamps on each spark chamber photo. A posteriori, once the range of the detected particle is known, a bidimensional analysis of the pulse height in S_2 and S_3 allows the remaining $\sim 10\%$ contamination of pions and electrons to be eliminated completely.

While criteria *a*) and *d*) were always used, criteria *b*) and *c*) were used alternatively, according to which proton energy was explored. Sometimes, for intermediate proton energies both criteria *b*) and *c*) were used, the first one for particles stopping in SC_1 and SC_2 (fig. 2), and the second one for particles stopping in SC_3 and SC_4. In this case, the spark chambers were triggered by the coincidence:

$$N_1 = S_0\,(S_1\,D)\,S_2\,S_3\,\bar{S}_4 \qquad \text{or} \qquad N_2 = S_0\,S_1\,S_2\,S_3\,S_4\,\bar{C}p$$

($S_1\,D$ means discrimination on S_1 ; bar indicates an anticoincidence).

For this reason counter S_4 was put in the telescope: it is of course switched-off when only one of criteria *b*) or *c*) is applied.

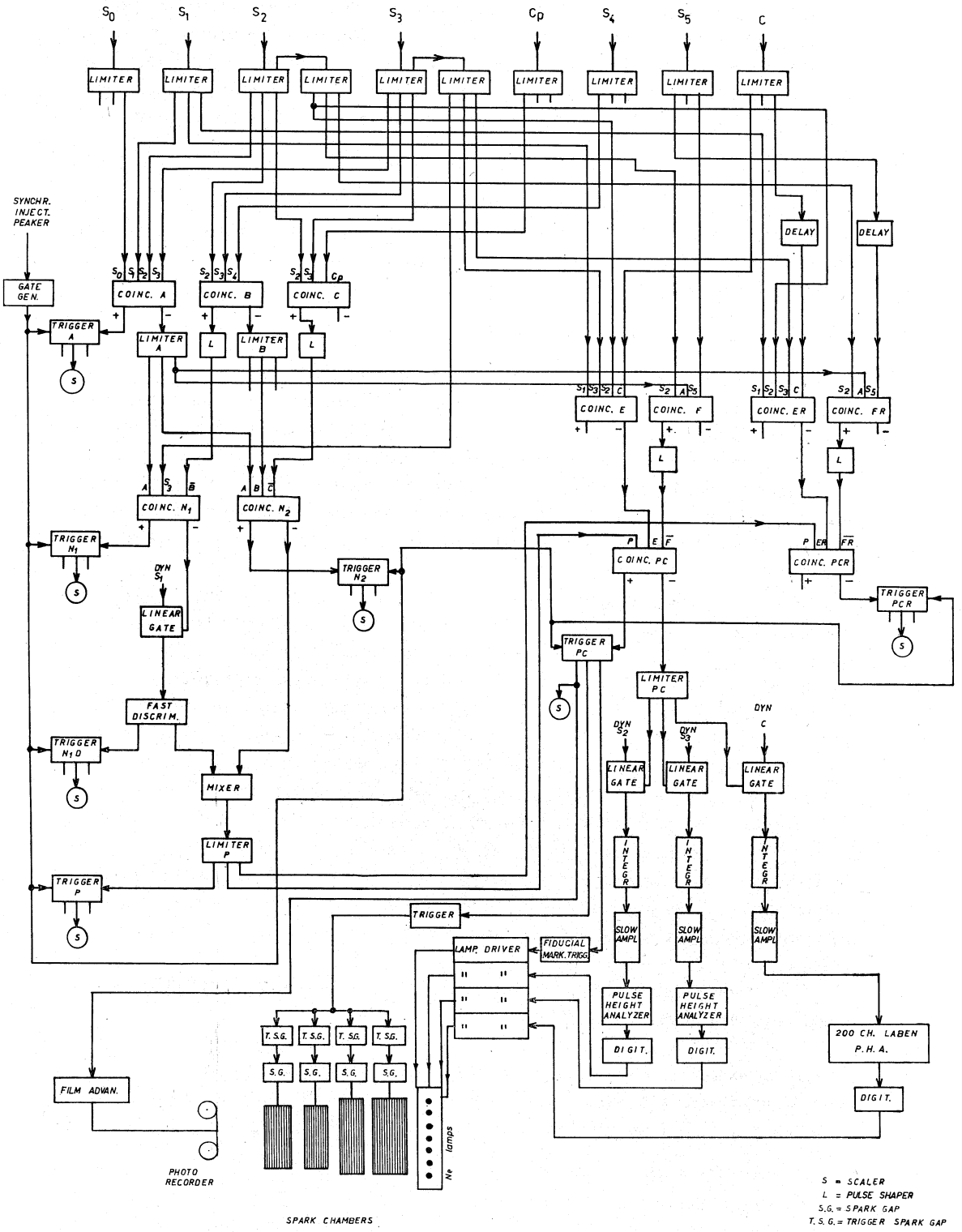


Fig. 3. – Block diagram of the electronics.

The pulse height of C is also recorded on each spark chamber photo, allowing to check that we are not losing $\pi^{0\prime}s$ due to a threshold on it.

The part of the electronics concerning the coincidence of a γ–ray with a proton has been duplicated (fig. 3), in order to obtain a simultaneous measurement of the accidental rate, which was however, in this measurement, of the order of 5%.

CONTAMINATION FROM OTHER PROCESSES.—The main processes in competion with process (1) are the Compton effect on proton (elastic scattering of γ–rays) and the multipion photoproduction.

The Compton effect:

$$\gamma + p \rightarrow \gamma + p \tag{2}$$

is hardly distinguishable from single π^0 photoproduction, since the kinematics of the two reactions are very similar. However, the cross-section for elastic scattering of photons [12] is $\sim 2\%$ of the cross-section for process (1). Since the efficiency of our γ–telescope to detect the γ–ray from process (2) is $\sim 100\%$, while the efficiency of detection of the π^0 from process (1) is $\sim 50\%$, there is in our results a contamination of $\sim 4\%$ from process (2). We have not attempted to separate this contamination, which thus affects our results.

The multipion photoproduction can also simulate in our apparatus events from reaction (1). However, there is a region which is kinematically free of events of this kind: this region corresponds to incident photons whose energy lies in an interval of $\sim$ 140 MeV below the maximum energy of the bremsstrahlung spectrum. In our measurements, the energy of the machine was always such that the energy region explored by the spark chambers was free of multipion photoproduction: the energy spectrum of protons from reaction (1) is an image (weighted with the cross-section for process (1)) of the bremsstrahlung spectrum. Properly choosing the absorbers in the proton telescope, the step in the proton energy distribution, corresponding to the end of the bremsstrahlung spectrum [9], was always put within the energy range explored by the spark chambers; the range of photon energy to which each measurement refers extends less than $\sim$ 140 MeV below the maximum energy.

The events we measure are thus due only to process (1), with a small contamination from process (2).

ELABORATION OF THE DATA; RESULTS.—When a coincidence of the proton telescope with the γ–telescope occurs, we get thus a photo which contains the following information:

entrance point (angle) of the proton;
range (energy) of the proton;
pulse height in counters S_2, S_3, C.

When analyzing the photos, this information is transferred on punched cards, which are then analyzed by an IBM 1620 computer. Photos which do not contain a track are disregarded: they correspond to particles which stop in counter S_3 or in the first plate of SC_1, or to accidental triggers.

Particles interacting in the plates of the chambers are accepted, unless the secondaries emitted are at angles $\geq 85^\circ$. In fact we applied to the final data a correction for nuclear interactions (see Appendix I), the mean free path for nuclear interactions having been extracted from measurements [13] made in bad geometry.

Photos containing two tracks are also disregarded: they are of the order of $1 \div 2\%$ of the photos, and the final data are corrected for this effect.

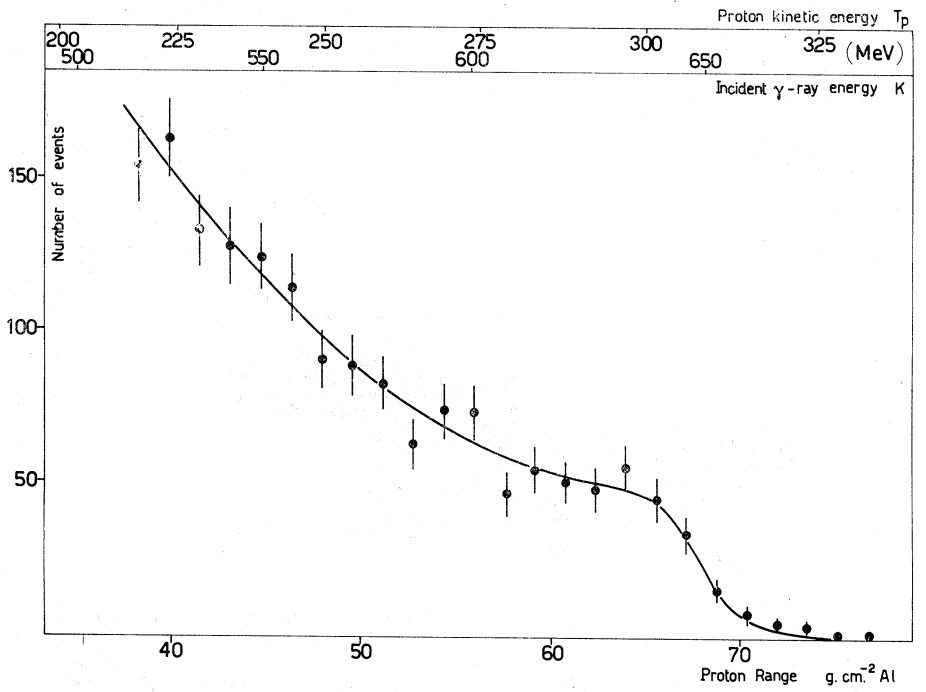


Fig. 4. – A proton spectrum as a function of the stopping gap (range).

The kinetic energy of the proton and energy of the photon producing the reaction $\gamma + p \rightarrow \pi^0 + p$ are also indicated (upper scales). The energy of the synchrotron was 650 MeV, and in correspondence a step in the proton spectrum appears (see text).

A bidimensional plot of the pulse heights in counters S_2 and S_3 allows us to eliminate, as we said, the pions and electrons from the accepted events.

After subtraction of the accidental rate and empty target background, the remaining events (protons stopping in the chambers in coincidence with a γ–ray in C) are plotted on a bidimensional graph in the variables R = range of the proton and E_γ = energy of the γ–ray in C.

The projection on the E_γ–axis allows us to check that we are not missing events due to a threshold on C, and that the energy distribution of the γ from the π^0, as computed by Montecarlo (see Appendix II), corresponds

to experimental spectrum. The projection n (R) on the R–axis, corrected for nuclear interactions, is transformed in a distribution N (Tp) as a function of the kinetic energy Tp of the protons (using the Berkeley range-energy tables), and used to determine the cross-section. In fig. 4 a typical spectrum n (R) is shown, with the step image of the bremsstrahlung spectrum.

The cross section is given by:

$$\frac{d\sigma}{d\Omega^* \cdot dK} = \frac{N(Tp) \cdot dTp/dK}{Q \cdot \frac{b(K/E_0)}{K} \cdot \varepsilon \cdot \left(\frac{d\Omega^*}{d\Omega}\right)_p \cdot \Delta\Omega \cdot n}$$

where:

Tp = kinetic energy of the proton;
K = energy of the incident photon;
N (Tp) = number of events per unit interval of Tp;
Q = number of equivalent quanta used to collect the data;
$\frac{b(K/E_0)}{K}$ = shape of the bremsstrahlung spectrum;
ε = efficiency of detection of the γ from the π^0 decay in C;
n = number of atoms/cm^2 of H_2 in the target;
$\Delta\Omega$ = solid angle of the proton telescope.

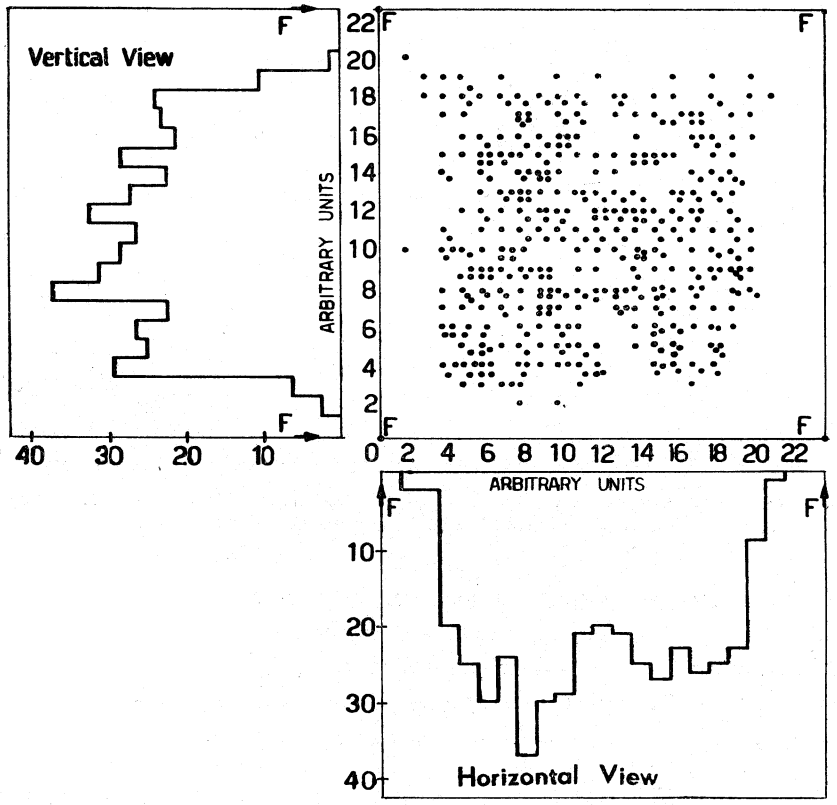


Fig. 5. – Distribution of the protons as a function of the entrance point in SC_1. The arrows (F) indicate the fiducial marks which delimit the useful region (31·5×31·5 cm^2). The proton distribution fits with the expected shadow of counter S_2 from the H_2 target.

The meaning of dTp/dK and of $d\Omega^*/d\Omega$ is obvious.

The solid angle $\Delta\Omega$ is S/r^2, where S in the area of counter S_3 and r its distance from the H_2 target. The loss due to multiple scattering was evaluated to be negligible. In addition, a check of this was obtained by making a distribution of the events as a function of the entrance point in the spark chamber SC_1, which appeared to be a rectangular distribution (fig. 5).

The results of our measurement are shown in fig. 6, and compared with the results already available in the same energy region [10]. The agreement is fairly close.

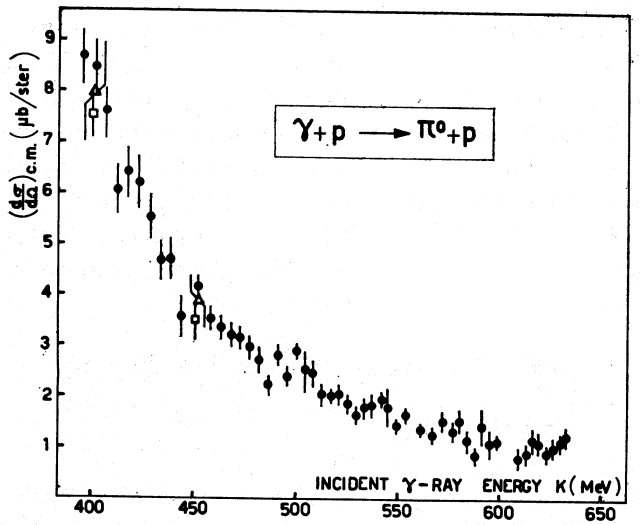


Fig. 6. – Experimental results; compared with the results already available in this energy region at the same angle:
● present experiment; △ V. S. MCDONALD et al. [10]; □ D. C. OAKLEY et al. [10].

The energy distribution unites fairly well the decrease of the first resonance and the rise of the second one. In the energy interval we explored with high resolution no evident shoulder or peak or bump appears clearly.

The P_{11} resonance, whose width as we said is very large, of the order of $\pm$ 100 MeV, would not appear in our data as a sharp bump, but rather as a flat background raising the level of the cross-section around 500–600 MeV where the valley of the distribution happens to be.

Just in this last respect the low experimental value of the minimum ($\sim$ 1 $\mu b/sr$) leaves a fairly small space for a high amplitude of P_{11} when any reasonable space is left to the tails of the neighbouring resonances.

In conclusion, apart from possible interferences, our preliminary results tend to show that the P_{11} should have a small contribution, if any, in single neutral pion photoproduction.

However, to get more definite conclusions, measurements at various angles are in progress in Frascati, whose results will be published shortly.

The authors want to stress that this work would not have been performed without the continuous interest, collaboration and advice of Prof. G. Salvini.

APPENDIX I.—*Correction to the proton spectrum due to nuclear interactions in the spark chambers.*

In addition to losing energy through ionization, protons can suffer nuclear interactions in the spark chambers. This results in a modification of the proton spectrum.

Measurements of the mean free path of interaction with monochromatic beams of protons have been made by different authors. We will use in the following the results of the experiment by G. P. Millburn et al. [13].

The results of this experiment can be interpreted as follows: if we call $\mathfrak{M}(X, R)$ the distribution of the stopping point (X) of monochromatic protons, disregarding the straggling and nuclear interaction, one should have $\mathfrak{M}(X, R) = \delta(X - R)$ (All the distribution functions will be normalized to 1). R depends on the energy of the beam. Taking into account the nuclear interactions, the distribution becomes:

$$\text{(I.1)} \qquad \begin{cases} \mathfrak{M}(X, R) = \frac{1}{\lambda} e^{-X/\lambda} + e^{-R/\lambda}\,\delta(X - R) & X \leq R \\ \mathfrak{M}(X, R) = 0 & X > R \end{cases}$$

if we use the criterion of assigning to the range X a particle interacting at X without charged secondaries, or interacting at a point $X' < X$ if one of the charged secondaries extends to a projected range X.

$\lambda = 110\, g/\mathrm{cm}^2$ if the stopping material is aluminum, and is constant for proton energies between 90 and ~ 250MeV [13].

If instead of a monochromatic incident beam, we have any spectrum N (R), due to nuclear interactions it becomes:

$$\text{(I.2)} \qquad M(X) = \int_0^\infty dR\, N(R)\, m(X, R).$$

By inserting (I.1) into (I.2) and integrating, we get:

$$\text{(I.3)} \qquad N(X) = M(X)\, e^{X/\lambda} - \frac{1}{\lambda} \int_X^\infty dR\, N(R).$$

Our problem is to get N (R) from (I.3). Deriving (I.3) with respect to X, we have:

$$\text{(I.4)} \qquad \frac{dN}{dX} - \frac{1}{\lambda} N(X) + \varphi(X) = 0$$

where

$$\varphi(X) = -e^{X/\lambda}\left(\frac{M(X)}{\lambda} + \frac{dM}{dX}\right).$$

The general solution of equation (I.4) is:

$$N(X) = e^{X/\lambda}\left[N(X_0)\, e^{-X_0/\lambda} + M(X) - M(X_0) + \frac{1}{\lambda}\int_{X_0}^{X} dS\, M(S)\right]. \tag{I.5}$$

The parameter X_0 is an arbitrary parameter which must be determined by the boundary condition. It turns out that X_0 can be taken as any value of X large enough so that $N(X_0)=0$ and as a consequence $M(X_0)=0$; for instance $X_0 = +\infty$.

(I.5) reads then:

$$N(X) = e^{X/\lambda}\left[M(X) - \frac{1}{\lambda}\int_{X}^{\infty} dS\, M(S)\right] \tag{I.6}$$

which is the required solution.

Integrating (I.6) over the thickness ΔR of one spark chamber plate, and assuming that N (X) is fairly constant in this interval we get:

$$N(R) = \int_{R}^{R+\Delta R} dX\, N(X) = e^{R/\lambda}\left[\Delta M(R) - \frac{\Delta R}{\lambda}\sum_{\geq R}\Delta M(R)\right]$$

where:

$\Delta M(R)$ = number of measured events at the gap corresponding to a range between R e $R + \Delta R$;

$\sum_{\geq R}\Delta M(R)$ = number of measured events with a range $\geq R$;

$\Delta N(R)$ = number of events expected to stop at the considered gap in the absence of nuclear interactions.

APPENDIX II.—*Calculation of the geometrical efficiency of detection of the process* $\gamma + p \rightarrow \pi^0 + p$ *by the Montecarlo method.*

Of all reactions (1) occurring in the target, only a part is detected by the experimental apparatus: in fact, in order that a reaction (1) be detected, it is necessary that the proton enters the proton telescope, and that at least one of the γ–rays from the π^0 decay enters C. It is easy to see that in our kinematical conditions it is not possible that both γ–rays from the π^0 decay enter C, since its angular aperture is smaller than the minimum angle between the two γ–rays.

The probability that process (1) be detected by our apparatus, has been calculated with the Montecarlo method using the computer IBM 7040

of the Istituto Superiore di Sanità of Rome. The block diagram of this calculation is shown in fig. 7.

The imput data are:

K = energy of the incident photon;
θ_c = angle between the direction of γ–rays beam, and the direction from the center of the H_2 target to the center of C;
$\Delta\theta_c$ = angular aperture of C;
θ_p^{min}, φ_p^{min}, θ_p^{max}, φ_p^{max} = minimum and maximum angles accepted by the proton telescope.

Starred symbols (e.g. θ^*) refer to the center of mass system (c.m.s.) of reaction (1); crossed symbols (e.g. θ_γ^+) refer to the remaining system of the π^0; symbols without index refer to the laboratory system (l.s.).

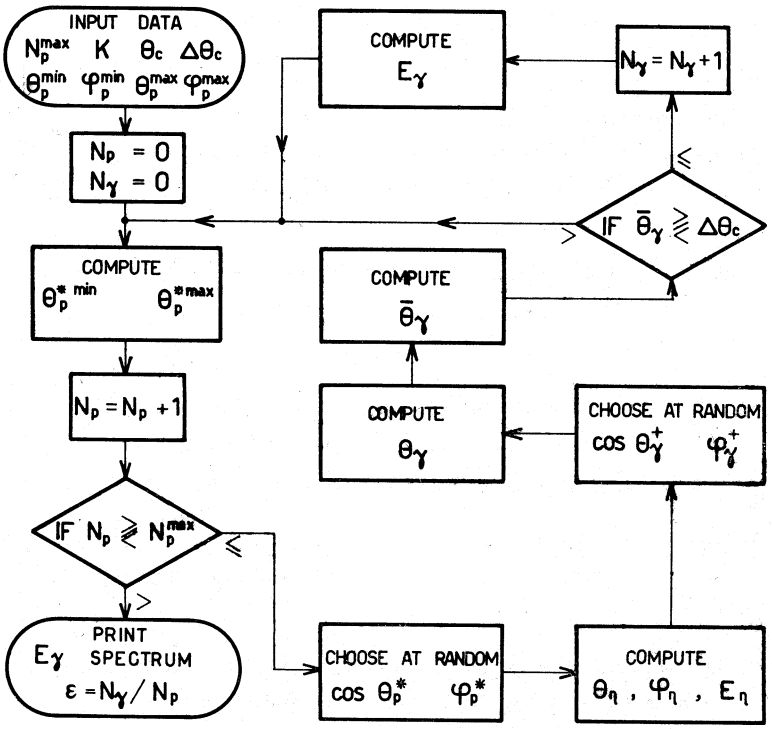


Fig. 7. – Block diagram of the Montecarlo calculation of the efficiency of C to detect the π^0 from reaction (1).

The calculation is performed as follows:

1) The minimum and maximum angles of the proton telescope in the c.m.s. are calculated.

2) cos θ_p^* and $\varphi_p^* \equiv \varphi_p$ are randomly sorted within those limits. The distribution is supposed constant in this small interval.

3) The vector $\vec{p}_{\pi^0}$ momentum of the π^0, is calcuated.

4) $\cos\theta_\gamma^+$ and $\varphi_\gamma^+ \equiv \varphi_\gamma$ are sorted with flat distribution in the total solid angle. θ_γ^+ is the angle between the direction of the γ in the π^0 rest system and the line of flight of the π^0. $\varphi_\gamma^+ \equiv \varphi_\gamma$ is measured with respect to a plane passing through the center of C, and the line of flight of the π^0.

5) The angle $\cos\theta_\gamma^+$ is transformed to the laboratory system.

6) The angular distance $\bar{\theta}_\gamma$ between the center of C and the decay γ is computed.

7) $\bar{\theta}_\gamma$ is compared with $\Delta\theta_c$; if $\Delta\theta_c < \bar{\theta}_\gamma$ the event is not accepted. If $\Delta\theta_c \geq \bar{\theta}_\gamma$ the event is detected by C and thus accepted.

8) The energy E_γ of the detected γ is computed and memorized.

9) The spectrum of E_γ is plotted.

The calculation is repeated until good enough statistics are collected. Since the efficiency turns out to be $\sim 50\%$, if we repeat the calculation 50,000 times, we get the efficiency ε with an error of $\sim 0.5\%$.

In fig. 8 the efficiency as a function of K is shown.

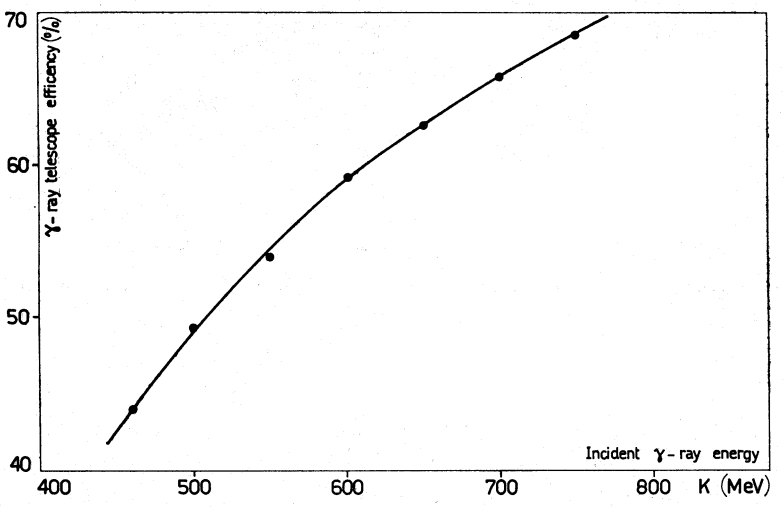


Fig. 8. – Result of the Montecarlo calculation: efficiency of detection of the π^0 from reaction (1) as a function of the energy of the incident photon.

APPENDIX III.—*Calibration of the Cerenkov* C.

The Cerenkov counter C (fig. 2) is a solid glass cylinder. The lead glass is viewed by three Philips 58 AVP, 5″ photomultipliers connected in parallel. At the entrance of the Cerenkov a lead ring fixes the aperture of the counter towards the H_2 target to a diameter of 25 cm.

The calibration of the lead glass Cerenkov has been done by sending to C a beam of monochromatic electrons at various energies. The beam was taken at the exit of the Frascati pair spectrometer [11]. This calibration

has been considered as valid for the photons. In fact the initial difference (a photon rather than an electron) will only presumably display the development of the shower in the lead glass, while the length of our Cerenkov ($\sim$ 12 radiation lengths) is enough to absorb all the cascade shower in the range of energies (200–700 MeV) covered in our measurements.

Experimental disposition for the calibration.

The disposition for the calibration is given in fig. 9. The bremsstrahlung spectrum from the synchrotron (the energy of the machine was set at 1000 MeV) is collimated in the lead collimators C_1 and C_2. Use is made of a sweeping magnet M to eliminate contaminating electrons in the beam. The bremsstrahlung beam travels in a vacuum on the way from M to the con-

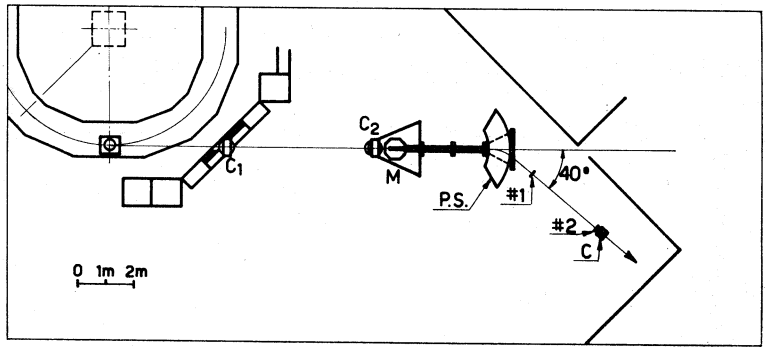


Fig. 9. – Experimental arrangement for the calibration of C.

C_1, C_2: lead collimators; M: sweeping magnet; P. S.: pair spectrometer; 1, 2: scintillation counters; C: Cerenkov.

verter. The gap of the spectrometer is also under vacuum. The converter producing the electron pairs at the entrance of the spectrometer is an aluminum disk of thickness varying from 0.1 to 1 mm (0.1 mm in the case of fig. 10). Once the Cerenkov was placed at a given exit angle θ from the spectrometer the energy of the electrons hitting the Cerenkov was changed by varying the magnetic field in the spectrometer. The angle θ is fixed at 40° by the counters 1 (10×10 cm^2) and 2 (5×5 cm^2) (fig. 9). In these conditions the spectrum of the electrons entering the Cerenkov is fairly well defined around the average energy E: in fact it is flat with a $\delta E/E = \pm 2\%$.

All the electronics used in the calibration, from the Cerenkov to the analyzer, were the same as we employed with the actual measurement of the π^0.

Results of the calibration.

The pulse height distributions from the Cerenkov are shown in fig. 10 for different energies of the electron beam. We see, as expected, that the abscissae of the peaks of these distributions are linearly correlated to the

energy of the electron beam entering the Cerenkov. This appears clearly in fig. 11 where the peak position in the multichannel is plotted versus the electron energy.

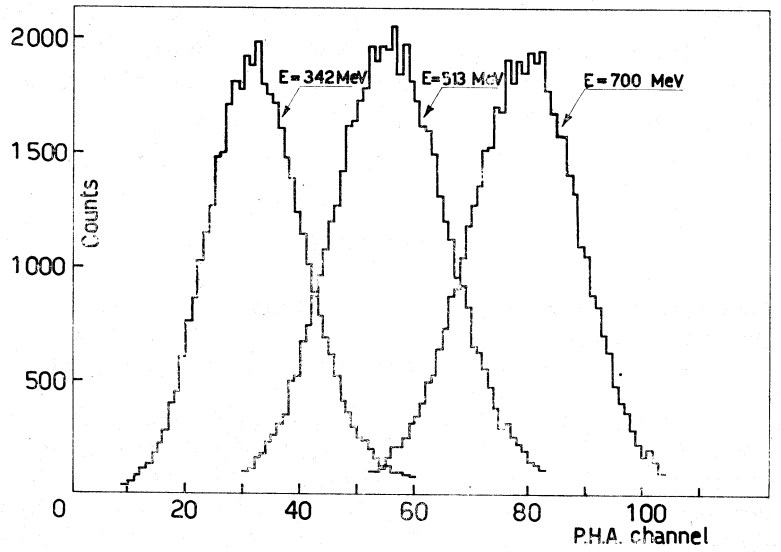


Fig. 10. – Typical pulse height distribution from C, corresponding to different energies of the incident electrons.

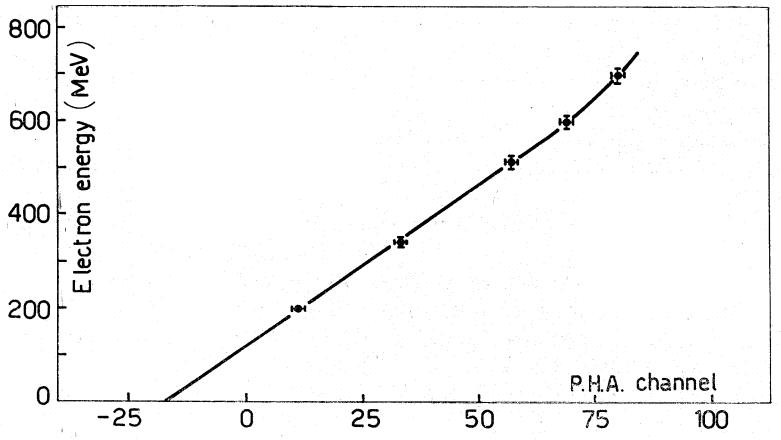


Fig. 11. – Average pulse height from C, as a function of the energy of the incident electrons.

As we can estimate from fig. 10, the relative width $\Delta E/E$ of the pulse height spectrum is always less than $\pm$ 30%. The values of the absolute widths ΔE fix the resolution of the Cerenkov C at each energy. By illuminating with electrons different regions of the Cerenkov C and by slightly rotating the axis of the Cerenkov with respect to incident beam, we verified that each pulse height distribution of fig. 10 did not change appreciably.

Stability of the Cerenkov calibration.

By repeating our calibration with some regularity we found some slight ($< 10\%$) and slow variations of the calibration constants (position of the peak and width). These changes were taken continously under control and corrected by systematic measurements of the pulse height distribution of the cosmic ray particles hitting the Cerenkov.

References.

[1] A. Rosenfeld, A. Barbaro Galtieri, W. H. Barkas, P. L. Bastien, J. Kirz and M. Roos, UCRL–8030–Part I (March 1965).

[2] P. Bareyre, C. Bricman, G. Valladas, G. Villet, J. Bizard and J. Seguinot, « Physics Letters », *8*, 137 (1964).

[3] G. Cocconi, E. Lillethun, J. P. Scanlon, C. A. Stahlbrandt, C. C. Ting, J. Walters and A. M. Wetherell, « Physics Letters », *8*, 134 (1964); G. Bellettini, G. Cocconi, A. N. Diddens, E. Lillethun, J. P. Scanlon and A. M. Wetherell, *The production of nucleon isobars in high energy p—p and e—p collision*, Hamburg Conference (1965). G. Bellettini, G. Cocconi, A. N. Diddens, E. Lillethun, J. P. Scanlon, A. M. Shapiro, and A. M. Wetherell « Physics Letters » *18*, 167 (1965).

[4] S. L. Adelman, « Phys. Rev. Letters », *13*, 555 (1964).

[5] L. D. Roper, « Phys. Rev. Letters », *12*, 340 (1964); P. Auvil, A. Donnachie, A.T. Lea and C. Lovelace, « Physics Letters », *12*, 76 (1964); B.H. Bransden, P. J. O'Donnel and R. G. Moorhouse, « Physics Letters », *11*, 339 (1964); R. H. Dalitz and R. G. Moorhouse, « Physics Letters », *14*, 159 (1965).

[6] V. Montelatici, « Nuclear Instr. and Meth. », *29*, 121 (1964) and Frascati report LNF-62/20 (1962).

[7] R. R. Wilson, « Nuclear Instr. and Meth. », *1*, 101 (1959).

[8] C. Bacci, V. Bidoli, G. Salvini e M. Spinetti, Istituto di Fisica, Univ. di Roma, Nota interna n. 66 (30.11.1964).

[9] G. Diambrini, A. S. Figuera, B. Rispoli and A. Serra, « Nuovo Cimento », *19*, 250 (1961).

[10] D. C. Oakley and R. L. Walker, « Phys. Rev. », *97*, 1283 (1955); W. S. McDonald, V. Z. Peterson and D. R. Corson, « Phys. Rev. », *107*, 577 (1957); J. I. Vette, « Phys. Rev. », *111*, 622 (1958); H. De Staebler Jr., E.F. Erickson, A. C. Hearn and C. Schaerf, « Phys. Rev. », to be published.

[11] G. Bologna, G. Diambrini and G. P. Murtas, « Suppl. Nuovo Cimento », *24*, 342 (1962).

[12] R. F. Stiening, E. Loh, and M. Deutsch « Phys. Rev. Letters », *10*, 536 (1963).

[13] G. P. Millburn, W. Birnbaum, W. E. Crandall and L. Schecter, « Phys. Rev. », *95*, 1268 (1954).

RIASSUNTO. — Si descrivono il dispositivo e il metodo sperimentale utilizzati in una misura della sezione d'urto per la reazione $\gamma + p \rightarrow \pi^0 + p$. Questa misura è stata eseguita all'elettrosincrotrone di Frascati da 1,1 GeV, e si riferisce ad una energia dei fotoni primari compresa fra 400 e 600 MeV, e ad un angolo del π^0 del baricentro di 135°. La principale caratteristica del dispositivo sperimentale, formato di contatori di Cerenkov e a scintillazione e di camere a scintilla, è la buona risoluzione in energia del fotone incidente ($\sim \pm 5$ MeV) quale è richiesta per mettere in evidenza eventuali risonanze strette, con una larghezza dell'ordine di alcune decine di MeV.

I risultati mostrano un andamento regolare della sezione d'urto in funzione dell'energia. In particolare non si trova alcuna indicazione in favore della risonanza P_{11}, che è stata trovata in altri canali di reazione. I pochi risultati sulla fotoproduzione già disponibili in questa regione cinematica, sono in buon accordo coi nostri risultati.